Band gap renormalization in n-type GeSn alloys made by ion implantation and flash lamp annealing

Prucnal, S.; Berencén, Y.; Wang, M.; Rebohle, L.; Kudrawiec, R.; Polak, M.; Zviagin, V.; Schmidt-Grund, R.; Grundmann, M.; Grenzer, J.; Turek, M.; Droździel, A.; Pyszniak, K.; Zuk, J.; Helm, M.; Skorupa, W.; Zhou, S.;

Originally published:

May 2019

Journal of Applied Physics 125(2019), 203115

DOI: https://doi.org/10.1063/1.5082889

Band gap renormalization in n-type GeSn alloys made by ion implantation and flash lamp annealing

S. Prucnal[1,*], Y. Berencén[1], M. Wang[1], L. Rebohle[1], R. Kudrawiec[2], M. Polak[2], V. Zviagin[3], R. Schmidt-Grund[3], M. Grundmann[3], J. Grenzer[1], M. Turek[4], A. Drożdziel[4], K. Pyszniak[4], J. Zuk[4], M. Helm[1], W. Skorupa[1] and S. Zhou[1]

[1]*Helmholtz-Zentrum Dresden-Rossendorf, Institute of Ion Beam Physics and Materials Research, Bautzner Landstrasse 400, 01328 Dresden, Germany*
[2]*Faculty of Fundamental Problems of Technology, Wroclaw University of Science and Technology, Wybrzeże Wyspiańskiego 27, 50-370 Wrocław, Poland*
[3] *Felix-Bloch-Institut für Festkörperphysik, Universität Leipzig Linnéstr. 5, 04103 Leipzig, Germany*
[4] *Maria Curie-Sklodowska University, Pl. M. Curie-Sklodowskiej 1, 20-035 Lublin, Poland*

* To whom correspondence should be addressed: s.prucnal@hzdr.de

Abstract

The last missing piece of the puzzle for the full functionalization of group IV optoelectronic devices is a direct-band-gap semiconductor made by CMOS compatible technology. Here we report on the fabrication of GeSn alloys with a Sn concentrations up to 4.5% using ion implantation followed by ms-range explosive solid phase epitaxy. The n-type single crystalline GeSn alloys are realized by co-implantation of Sn and P into Ge. Both the activation of P and the formation of GeSn are performed during a single-step flash lamp annealing for 3 ms. The band-gap engineering in GeSn as a function of the doping level and Sn concentration is theoretically predicted by density functional theory and experimentally verified using ellipsometric spectroscopy. We demonstrate that both the diffusion and the segregation of Sn and P atoms in Ge are fully supressed by ms-range non-equilibrium thermal processing.

Keywords: GeSn, ion implantation, flash lamp annealing, spectroscopic ellipsometry, XRD

Introduction

Nowadays more than 95% of electronic devices are made of Si. The lack of direct band gap group-IV semiconductors require the integration of foreign compound semiconductors like group III-V materials on the same Si platform. The integration of III-V compound semiconductors with Si can be realized by direct growth of III-V on Si (heteroepitaxy) or wafer bonding techniques [1, 2]. III-V compound semiconductors are appealing solutions to replace Si in CMOS technology for fabricating optical and electronic devices with much higher electron mobility than that in Si. However, before realizing a CMOS technology based on III-V compound semiconductors, many challenges have to be overcome such as a high density of interface states, the lack of stable gate oxides, the lack of low-resistance ohmic contacts, and high leakage current in FETs [3-5]. The ideal solution would be group-IV direct band gap semiconductors. Ge can be converted from an indirect to a direct band gap semiconductor using either ultra-high doping with electron concentrations above 8×10^{19} cm^{-3} or biaxial tensile strain above 1.7%, or alloying Ge with Sn with Sn concentrations higher than 8% for cubic GeSn alloys or using Ge nanostructures [6-13]. Recently, it was shown that Ge alloyed with Sn can become a direct band gap semiconductor and shows lasing for a Sn concentration higher than 12.5% [6]. All of the mentioned approaches are challenging, because n-type doping of Ge above 3×10^{19} cm^{-3} is metastable, the formation of strained Ge layers with a strain value higher than 0.5% is difficult and the equilibrium solid solubility of Sn in Ge is below 1%. Therefore, the direct-band-gap GeSn must be fabricated by non-equilibrium methods. The most common fabrication method for direct band gap GeSn is molecular beam epitaxy (MBE). It was shown that using MBE the GeSn alloy can be grown on Ge with a Sn content of up to 25% [14]. In addition, the grown GeSn layer can be in-situ doped with Sb or B to achieve either n-type or p-type conductivity, respectively. However, the fabrication of planar devices and in-situ doping using the MBE technique is strongly limited. The alternative method to MBE to form GeSn alloys, is high fluence ion implantation of Sn into Ge followed by thermal annealing [15].

In this work, we present the formation of heavily doped n-type GeSn alloys with a Sn content of up to 4.5 at.%. The Sn is incorporated into Ge using ion implantation followed by flash lamp annealing (FLA) for 3 ms. The n-type doping is realized by the co-implantation of P ions. The activation of the implanted P and the alloying of Sn with Ge take place during a single-pulse FLA step. The band gap of GeSn and the position of the Fermi level are theoretically predicted using density functional theory (DFT) and experimentally verified by near-infrared spectroscopic ellipsometry (SE). High resolution X-ray diffraction (HR-XRD) and Rutherford

backscattering spectrometry (RBS) were used to investigate the microstructural properties of the fabricated GeSn alloys.

Experimental part

The undoped (001) Ge wafers with resistivity higher than 50 Ωcm (intrinsic electron concentration $n_e < 6 \times 10^{13}$ cm^{-3}) were implanted either with Sn only or co-implanted with Sn and P ions. The Sn ions were implanted at an energy of 200 keV with two different fluences of 1.2×10^{16} cm^{-2} and 1.6×10^{16} cm^{-2} corresponding to a peak Sn concentration of 3 and 4.5 at.%, respectively. P was implanted at an energy of 80 keV with a fluence of 1×10^{15} cm^{-2} resulting in an overlapping depth distribution of Sn and P. To protect the Ge surface a 30 nm thick SiO_2 layer was deposited prior to ion implantation by plasma enhanced chemical vapor deposition. The SiO_2 capping layer was removed by buffered hydrofluoric acid after annealing. Moreover, during the ion implantation process the sample temperature was kept below -120 ^oC in order to mitigate the implantation-related damages. The annealing was performed using rear-side FLA for 3 ms at an energy density of 65 Jcm^{-2} [16, 17]. Prior to this step, the FLA samples were preheated at 180 ^oC for 60 s. The implanted layer recrystallizes via explosive solid phase epitaxy during the FLA pulse. The ion implantation parameters are summarised in Table 1.

The Sn and P distribution was simulated using SRIM code [18], and the thickness of GeSn layers was measured by RBS. The substitutional efficiency of Sn into the Ge lattice site was investigated using random and channeling Rutherford backscattering spectrometry (RBS/R and RBS/C). RBS was carried out using the 1.7 MeV He^+ beam of the Rossendorf van de Graff accelerator. The Sn profile was then calculated by the help of the RUMP program [19]. Since we know the Sn distribution in implanted and annealed layers the thickness of the GeSn layer and Sn concentration can be determined. The thickness of the undoped and n-type GeSn layers is about 60 nm. The band-gap change in GeSn alloys was determined by means of spectroscopic ellipsometry. The thin-film complex dielectric function was obtained using a variable-angle spectroscopic ellipsometry (VASE, J.A. Woollam Co.) in a polarizer-compensator-sample-analyzer configuration.

The concentration of carriers in the implanted and annealed samples was estimated from temperature-dependent Hall effect measurements in a van der Pauw configuration. The microstructural properties were studied by HR-XRD. The X-ray measurements were carried out using an empyrean diffractometer operated with Cu-K_α radiation; the diffractometer was equipped with a Göbel mirror and a channel-cut (Ge220) monochromator on the source side.

For the 2θ–θ scans a small slit in front of a point detector was used. The reciprocal space maps were carried out using an area detector.

Results and discussion

The band structure and the position of the Fermi energy were calculated for undoped and fully relaxed GeSn alloys at 0K within the density functional theory (DFT) with the use of the FP-LAPW WIEN2k code [20]. A 54-atom supercell (3x3x3 multiplication of the primitive diamond unit cell) was used, allowing the study of the alloy in 1.85% of Sn concentration intervals. Within the supercell, the Sn atoms were distributed according to special quasi-random structures (SQS) to approximate a perfect alloy [21]. A full geometry optimization was performed with the use of the GGA-WC [22] functional, while the electronic structure was calculated using the Tran and Blaha MBJLDA [23] functional to describe the band gap correctly. According to the theory, the minimum Sn content needed to convert strain-free GeSn from an indirect to a direct band gap semiconductor is in the range of 7±2%, but rises up to 13% for biaxial compressively strained layers [24]. We recently reported that according to the theoretical study, the direct band gap in intrinsic and fully relaxed GeSn can be obtained for 6.5% of Sn [25]. The minimum Sn content needed for the direct band gap formation in GeSn can be further reduced by high n-type doping. Figure 1a shows the shift of the Fermi energy within the conduction band minimum (CB) as a function of the doping level for GeSn alloys for two different Sn concentrations 3.7 and 5.55 at. %. In the lightly doped n-type Ge and GeSn alloys ($n_e < 5\times10^{18}$ cm^{-3}) the Burstein-Moss effect can be neglected, however, it may have a significant influence on the effective absorption edge (E_g) for an electron concentrations higher than 8×10^{19} cm^{-3} in a cubic Ge and GeSn alloys [26, 27]. According to our calculations shown in Fig. 1a, the GeSn alloy with 5.55 at.% of Sn becomes a quasi-direct band gap semiconductor for an electron concentration of about 1×10^{19} cm^{-3}. If the doping level increases above 7×10^{19} cm^{-3}, the GeSn alloy will become a degenerated and quasi-direct band gap semiconductor for Sn concentrations as low as 3%. The calculated band structure of fully relaxed $Ge_{0.963}Sn_{0.037}$ alloy shows that the Fermi level is located in the CB at the Γ point. The $Ge_{0.963}Sn_{0.037}$ alloy with $n_e > 8\times10^{19}$ cm^{-3} is a degenerated and direct band gap semiconductor (see Fig. 1b). The shift of the direct band gap in the GeSn alloy as a function of Sn concentration and doping level was investigated by near-infrared spectroscopic ellipsometry. Measurements were conducted at room temperature in the spectral range from 0.5 to 4.0 eV. The ellipsometry spectra were analyzed by a model consisting of a layer stack as follows: (from the bottom) the substrate, the GeSn or GeSnP film layer and a surface layer with a 50% mix of the dielectric function (DF)

of the top-most film and air. The optical constants of the modified thin layers were determined numerically by using a Kramers-Kronig consistent B-Spline approximation with a knot number choice approach described elsewhere [25]. The optical layer thickness showed a general agreement with the RBS measurement. The obtained fit agreed well with the experimental data with a mean square error (MSE) of less than 2.2. The reflected light was detected by a Si and InGaAs diode in the UV-VIS and NIR spectral range, respectively. Figure 2 (a) shows the plot of $(\alpha h\nu)^2$ vs. incident photon energy ($h\nu$) obtained from a virgin Ge wafer and Sn implanted Ge samples followed by FLA for 3 ms at an energy density of 65 Jcm^{-2}. The $(\alpha h\nu)^2$ vs. $h\nu$ corresponds to the direct band gap absorption close to the band edge. The direct-band-gap of virgin Ge and GeSn alloys can be obtained by extrapolating the experimental data fitting to the photon energy axis. A much more accurate determination of the direct band-gap was achieved by the extraction of the 2nd derivative of the imaginary part of the dielectric function around the E_0 transition (see Fig. 2b). We have studied the shift of the optical transition around the E_0 critical point in bulk Ge and GeSn alloys with and without n-type doping. The inset of Figure 2a shows the low energy part of the second derivative of the imaginary part of the dielectric function obtained from not intentionally doped and P doped GeSn alloys with 4.5 at.% of Sn. The direct band gap transition in intrinsic Ge extracted from the second derivative of the imaginary part of the dielectric function is found to be at about 0.81 eV which is in good agreement with literature [6]. In the case of GeSn, the direct band gap transition shows a red shift with increasing Sn content. For 3 at.% of Sn the heavy hole (hh) and the Γ valley transition is measured to be at 0.72 eV. The increase of the Sn concentration up to 4.5 at.% reduces the direct band gap transition down to 0.69 eV. In the fully relaxed GeSn alloys with 3 at.% or 4.5 % of Sn the theoretically predicted direct band gaps are expected to be at 0.69 eV and 0.67 eV, respectively [25, 27]. The significant difference between the experimental data of fabricated GeSn alloys and the theoretically predicted direct band gap transitions in a cubic GeSn for a given Sn concentration is due to build-up of biaxial compressive strain in the recrystallized layer. The blue shift of the band gap in comparison with the calculated values for relaxed alloys is about 30 meV for 3 at.% of Sn and about 20 meV for 4.5 at.%, respectively. The lattice parameter of Ge is much smaller than the lattice parameter of relaxed GeSn, and the lattice parameter of GeSn increases with increasing Sn content. Due to the fact that the implanted layer recrystallizes epitaxially on a Ge substrate, the in-plane lattice parameter mimics the lattice parameter of the Ge substrate. This causes the biaxial compressive strain in the fabricated GeSn layers. The compressive strain is responsible for the blue shift of the band gap of the fabricated GeSn alloys [28-30]. Lin *et al.* have shown that the band gap change under biaxial compressive

strain in GeSn alloys is in the range of -85meV/% [29]. If we assume that in our case the differences between the experimental and theoretical values of the direct band gap in GeSn are caused by the strain only, the compressive strain can be calculated. Using a band gap change of -85meV/%, the biaxial compressive strain is 0.35% and 0.23% for $Ge_{0.97}Sn_{0.03}$ and $Ge_{0.955}Sn_{0.045}$, respectively.

Figure 2b shows the change of the band gap in GeSn as a function of Sn content in the undoped and P-doped layer. The electron concentration in all P doped samples is in the range of 3×10^{19} cm^{-3} as estimated from the Hall effect measurements. In all cases the n-type doping leads to a red shift of the direct band gap. This is due to the band gap renormalization in heavily doped semiconductors [31, 32]. The existence of the band gap renormalization is a direct evidence for the formation of the highly doped n-type Ge and GeSn layers. The hole concentration in the undoped sample is measured to be around 9.5×10^{16} cm^{-3}. Holes in ion implanted Ge originate from point defects like Ge vacancies which are known to be shallow acceptors with the energy level located about 20 meV above the valence band maximum [33]. Figs. 2c and d show the Hall resistance as a function of magnetic field measured at 3K obtained from the undoped and P doped $Ge_{0.97}Sn_{0.03}$ samples. The type of carriers determines the slope of the curve. The positive and negative slopes correspond to the p-type and n-type layers, respectively. The Hall measurement using the van der Pauw technique allows determining the sheet carrier density (n_s) by measuring the Hall voltage (V_H). If the thickness of the conductive layer (d) is known, the carrier concentration (n_e) can then be calculated according to the formula:

$$n_e = n_s/d\times k \qquad (1),$$

where k is the slope coefficient; positive for holes and negative for electrons. The inset in Fig. 2b shows the sheet resistance (SR) as a function of temperature obtained for undoped $Ge_{0.97}Sn_{0.03}$ and P doped samples. The SR of undoped $Ge_{0.97}Sn_{0.03}$ layer increases with decreasing temperature that is expected for intrinsic or lightly doped semiconductors. In the case of P doped sample, the SR shows small fluctuation in the temperature range from 200 K to 300 K and next slightly decreases with decreasing temperature. The decrease of the SR with decreasing temperature is typical for heavily doped semiconductors that exhibit metallic-like behavior [17].

The strain engineering and the lattice parameter change in GeSn alloys were investigated by XRD and micro-Raman spectroscopy. The XRD θ-2θ scans at the (004) reflection and reciprocal space maps (004, 224) provide information about the in-plane and out-

of-plane strain distribution in the fabricated GeSn films. Figures 3a and b show θ-2θ scans for two samples with different Sn concentrations. After the implantation and annealing an additional peak and thickness oscillations appeared at the low angle side of the Ge(004) substrate reflection describing an out-off-plane lattice expansion along [001].

The shift of the diffraction peak increases with increasing Sn concentration due to the expansion of the out-of-plane lattice parameter (compare Fig. 3a and 3b). The insets in the figs. 3a and b show the Sn distribution in the GeSn alloys extracted from XRD data. Even if we assume no Sn diffusion during the FLA process, the formation of end-of-range defects during implantation and a non-box like implantation profile of the Sn atoms leads to a slow decay of the out-of-plane strain at larger sample depths. The reciprocal space maps (Fig. 3c, d: $Ge_{0.97}Sn_{0.03}$) reveal that the in-plane lattice parameter of the GeSn corresponds to that of the Ge substrate. i.e. the system is fully biaxial compressive strained. The RSM is at the (224) reflection of the sample with a nominally Sn concentration of about 4.5% (Fig. 3e, f: $Ge_{0.955}Sn_{0.045}$) shows an onset of relaxation that has to be attributed to the upper most layer. Correspondingly, the estimated Sn concentration calculated from the simulation is slightly underestimated. The orange circles marked in the RSM images correspond to the expected position for Ge and GeSn alloys, either completely relaxed or fully strained. The strain relaxation towards the surface is consistent with the ellipsometry results. In case of P co-doped GeSn alloys the XRD does not show a change of the lattice parameter and the strain distribution due to the doping. In fact, the covalent radius of P is much smaller than that of Sn, but the P concentration is too small to significantly affect the strain in the fabricated layer. Moreover, the electronic contribution that normally expands the lattice will compensate any changes in the lattice parameter at this doping level [34].

Figure 4 shows the Raman spectra obtained in backscattering geometry for the implanted and annealed samples. The peak position of the transverse optical (TO) phonon mode shifts to smaller wavenumbers with increasing Sn concentration [35, 36]. For the sample with 3% of Sn, the TO phonon mode of Ge-Ge is located at 299.4 cm^{-1} and for 4.5 % the TO phonon mode shifts to 296.0 cm^{-1}. The Raman spectroscopy, similar to XRD, can be used to determine the composition and strain distribution in compound semiconductors. In relaxed GeSn, the shift of the peak position of the Ge-Ge Raman active phonon mode is caused by the mass difference (Ge vs. much heavier Sn) and the bond distortion (Ge-Ge bond vs. the much longer Ge-Sn bond). In fully relaxed $Ge_{1-x}Sn_x$ the shift ($\Delta\omega$) of the peak position of the TO phonon mode can be calculated according to [37]:

$\Delta\omega = \omega_{GeSn} - \omega_{Ge} = c \times x_{Sn}$ (2),

where ω_{GeSn} and ω_{Ge} are the TO phonon modes in relaxed GeSn and intrinsic Ge, respectively. x_{Sn} is the Sn concentration in GeSn alloys and c=-82.8 after Ref. 35. Since the experimental peak position of the TO phonon mode and the Sn concentration in GeSn are known, the strain in the investigated layer can be deduced. In general, a peak shift of the phonon mode towards smaller wavenumbers indicates tensile strain while a peak shift towards higher wavenumbers is caused by compressive strain. In particular, the *in-plane* strain ε for a given Sn content can be calculated according to

$\Delta\omega_{strain} = a \times x_{Sn} + b \times \varepsilon$ (3),

where ε is the biaxial strain, a=-83.11 and b=-374.53, and $\Delta\omega_{strain}$ is the shift of the TO phonon mode position with respect to the relaxed GeSn [37]. In our case $\Delta\omega_{strain}$ is 1.4 cm^{-1} for $Ge_{0.97}Sn_{0.03}$ and 0.7 cm^{-1} for $Ge_{0.955}Sn_{0.045}$ which correspond to a biaxial compressive strain of $\varepsilon_{||}$= -0.46% and $\varepsilon_{||}$=-0.26%, respectively. The compressive strain values obtained from Raman spectroscopy are similar to the values obtained from SE and in turn consistent with the XRD results. For $Ge_{0.97}Sn_{0.03}$ and $Ge_{0.955}Sn_{0.045}$ the average $\varepsilon_{||}$ derived from XRD is - 0.45% and -0.66%. In $Ge_{0.955}Sn_{0.045}$ sample the biaxial compressive strain decreases when approaching the surface. In figure 3f a weak intensity streak along the relaxation triangle (marked by dots) can be found. The orange cross marks the position corresponding to an in-plane strain of -0.26% and is perfectly placed within this intensity streak. Raman spectroscopy probes effectively only the first 30nm of the GeSn layer and is therefore only sensitive for this partially relaxed surface layer. Consequently the average strain estimated from the Raman spectra is much smaller (-0.26%) than that (-0.66%) measured over the entire layer by XRD.

In order to clarify the lattice position of Sn in the as-implanted sample and after FLA we have performed RBS spectrometry in random and channeling directions. Figure 5 shows the RBS/R spectrum obtained from as-implanted $Ge_{0.955}Sn_{0.045}$ and RBS/C spectra from as-implanted $Ge_{0.955}Sn_{0.045}$, from annealed $Ge_{0.955}Sn_{0.045}$, and from virgin Ge. The RBS/C data obtained from as-implanted samples are used to calculate the thickness of the implanted layer. We found that the damaged layer created during ion implantation is 110 nm thick while the GeSn layer is about 60 nm thick. The difference between the damaged layer and the Sn distribution is due to the generation of end-of-range defects during ion implantation [38].

In order to determine the concentration of Sn atoms in a substitutional position in annealed samples, the yield ratio χ_{min} between the random and the channelling spectra was calculated.

The energy range between 1380 and 1480 keV corresponds to the detected α particles backscattered by the Sn atoms. The χ_{min} value for Ge and Sn in the implanted sample is in the range of 7.8% and 10.5%, respectively. This means that more than 95% of Sn atoms are substituting the Ge lattice sites. It was shown that the maximum Sn concentration which can be implanted into Ge without porous formation is in the range of 15 at.% [15]. But the solubility of Sn in Ge is about thirty times lower [39] which makes such system extremely difficult to recrystallize without secondary phase formation e.g. Sn clusters. Moreover, we have to consider the recoil implantation of elements from capping layer into Ge [40]. Using SiO_2 capping both O and Si will be co-implanted into Ge. Here the most critical is oxygen that incorporated into Ge degrades the optical and electrical properties of Ge and GeSn alloys. For low and middle fluences of Sn implanted through the SiO_2 capping layer the O concentration recoil-implanted into Ge can be neglected. But for the high Sn fluence (Sn concentration > 6 at.%) oxygen co-implanted into Ge can form oxide clusters. Therefore for the formation of $Ge_{1-x}Sn_x$ alloys with x > 6at.% using ion implantation followed by non-equilibrium thermal processing alternative capping layers must be considered e.g. amorphous Si. Using amorphous Si, Si recoil implanted into Ge should increase the solid solubility of Sn in the Ge matrix and partially compensate the biaxial compressive strain.

Conclusions

We have fabricated single crystalline n-type GeSn with Sn concentrations up to 4.5%. A band gap renormalization has been observed after non-equilibrium processing consisting of ion implantation followed by FLA. We have demonstrated that the use of rear side FLA allows one to suppress the diffusion and segregation of Sn in Ge and in turn enables the incorporation of Sn into Ge in concentrations one order of magnitude higher than the equilibrium solid solubility. The ms-range rear side FLA is proven to be a powerful tool for the recrystallization of metastable systems with impurity concentrations much above the solid solubility. Our results present an approach toward direct bandgap group IV semiconductors.

Acknowledgment

Support by the Ion Beam Center (IBC) at HZDR is gratefully acknowledged. We would like to thank Andrea Scholz for XRD measurements This work was partially supported by the German Academic Exchange Service (DAAD, Project-ID:57216326) and the National Science Centre,

Poland, under Grant No. 2016/23/B/ST7/03451. Y. Berencén would like to thank the Alexander-von-Humboldt foundation for providing a postdoctoral fellowship.

References:

1. G. Roelkens *et al.*, *ACS Photonics* **3**, 969-1004 (2015).
2. Y. Jhang, K. Tanabe, S. Iwamoto, Y. Arakawa, *IEEE Photon. Technol. Lett*. **27**, 875 (2015).
3. S. Prucnal, S. Facsko, C. Baumgart, H. Schmidt, M. O. Liedke, L. Rebohle, A. Shalimov, H. Reuther, A. Kanjilal, A. Muecklich, M. Helm, J. Zuk, and W. Skorupa, *Nano Lett.* **11**, 2814 (2011).
4. D.-M. Geum, M.-S. Park, J. Y. Lim, H.-D. Yang, J. D. Song, C. Z. Kim, E. Yoon, S. H. Kim, and W. J. Choi, *Sci. Rep.* **6**, 20610 (2016).
5. M. T. Bjoerk, H. Schmid, C. D. Bessire, K. E. Moselund, H. Ghoneim, S. Karg, E. Loertscher, and H. Riel, *Appl. Phys. Lett*, **97**, 163501 (2010).
6. S. Wirths, R. Geiger, N. von den Driesch, G. Mussler, T. Stoica, S. Mantl, Z. Ikonic, M. Luysberg, S. Chiussi, J. M. Hartmann, H. Sigg, J. Faist, D. Buca, and D. Grützmacher, *Nat. Photon.* **9**, 88 (2015).
7. J. Liu, L. C. Kimerling, and J. Michel, *Semicond. Sci. Technol*. **27**, 094006 (2012).
8. S. Prucnal, J. Frigerio, E. Napolitani, A. Ballabio, Y. Berencén, L. Rebohle, M. Wang, R. Böttger, M. Voelskow, G. Isella, R. Hübner, M. Helm, S. Zhou and W. Skorupa, *Semicond. Sci. Technol.* **32**, 115006 (2017).
9. J. Liu, X. Sun, D. Pan, X. Wang, L. C. Kimerling, T. L. Koch, and J. Michel, *Opt. Express* **15**, 11272 (2007).
10. S. Biswas, J. Doherty, D. Saladukha, Q. Ramasse, D. Majumdar, M. Upmanyu, A. Singha, T. Ochalski, M. A. Morris, and J. D. Holmes, *Nat Commun*. **7**, 11405 (2016).
11. L. Augel, I. A. Fischer, F. Hornung, M. Dressel, A. Berrier, M. Oehme, and J. Schulze, *Opt. Letters* **41**, 4398 (2016).
12. M. Grydlik, F. Hackl, H. Groiss, M. Glaser, A. Halilovic, T. Fromherz, W. Jantsch, F. Schäffler, and M. Brehm, *ACS Photonics*, **3**, 298 (2016).
13. P. Rauter, L. Spindlberger, F. Schäffler, T. Fromherz, J. Freund, and M. Brehm, *ACS Photonics* **5**, 431 (2018).
14. M. Oehme, K. Kostecki, M. Schmid, F. Oliveira, E. Kasper, and J. Schulze, *Thin Solid Films* **557**, 169 (2014).
15. T. T. Tran, H. S. Alkhaldi, H. H. Gandhi, D. Pastor, L. Q. Huston, J. Wong-Leung, M. J. Aziz, and J. S. Williams, *Appl. Phys. Lett.* **109**, 082106 (2016).
16. S. Prucnal, L. Rebohle, and W. Skorupa, *Mater. Sci. Semicond. Process*, **62**, 115 (2017).

17. S. Prucnal, F. Liu, M. Voelskow, L. Vines, L. Rebohle, D. Lang, Y. Berencén, S. Andric, R. Boettger, M. Helm, S. Zhou and W. Skorupa, *Sci. Rep*. **6**, 27643 (2016).
18. J. F. Ziegler, J. P. Biersack, and U. Littmark, The Stopping and Range of Ions in Matter. New York: Pergamon Press. ISBN 978-0-08-021607-2 (1985).
19. L. R. Doolittle, Nucl. Instrum. Methods B 9, 344 (1985).
20. D. V. Likhachev, *Thin Solid Films* **636**, 519 (2017).
21. J. P. Perdew, K. Burke, and M. Ernzerhof, *Phys. Rev. Lett.* 77, 3865 (1996).
22. O. Rubel, A. Bokhanchuk, S. J. Ahmed, and E. Assmann, *Phys. Rev. B* **90**, 115202 (2014).
23. F. Tran, and P. Blaha, *Phys. Rev. Lett.* **102**, 226401 (2009).
24. S. Wirths, D. Stange, M.-A. Pampillón, A. T. Tiedemann, G. Mussler, A. Fox, U. Breuer, B. Baert, E. San Andrés, N. D. Nguyen, J.-M. Hartmann, Z. Ikonic, S. Mantl, and Dan Buca, *ACS Appl. Mater. Interfaces* **7**, 62 (2015).
25. M. P. Polak, P. Scharoch, and R. Kudrawiec, *J. Phys. D: Appl. Phys*. **50**, 195103 (2017).
26. R. Koerner, I. A. Fischer, D. Schwarz, C. Clausen, M. Oehme, and J. Schulze, *Semicond. Sci. Technol.* **32**, 124005 (2017).
27. S. Zaima, O. Nakatsuka, N. Taoka, M. Kurosawa, W. Takeuchi, and M. Sakashita, *Sci. Technol. Adv. Mater.* **16**, 043502 (2015).
28. F. Dybała, K. Żelazna, H. Maczko, M. Gladysiewicz, J. Misiewicz, R. Kudrawiec, H. Lin, R. Chen, C. Shang, Y. Huo, T. I. Kamins, and J. S. Harris, *J. Appl. Phys*. **119**, 215703 (2016).
29. C.-Y. Lin, H.-Y. Ye, F.-L. Lu, H. S. L, and C. W. Liu, *Opt. Mat. Express* **8**, 2795 (2018).
30. C. Eckhardt, K. Hummer, and G. Kresse, *Phys. Rev. B* **89**, 165201 (2014).
31. A. Walsh, J. L. F. Da Silva, and S.-H. Wie, *Phys. Rev. B* **78**, 075211 (2008).
32. G. Grzybowski, R. Roucka, J. Mathews, R. T. Beeler, J. Kouvetakis and J. Menéndez *Phys. Rev. B* **84**, 205307 (2011).
33. P. Śpiewak, J. Vanhellemont, K. Sueoka, K. J. Kurzydłowski,and I. Romandic, J. Appl. Phys. 103, 086103 (2008).
34. C. Xu, C. L. Senaratne, J. Kouvetakis, and J. Menendez, *Phys. Rev. B* **93**, 041201 (2016).
35. S. Prucnal, Y. Berencén, M. Wang, L. Rebohle, R. Böttger, I. A. Fischer, L. Augel, M. Oehme, J. Schulze, M. Voelskow, M. Helm, W. Skorupa, and S. Zhou, *Semicond. Sci. Technol.* **33**, 065008 (2018).
36. K. Gao, S. Prucnal, R. Huebner, C. Baehtz, I. Skorupa, Y. Wang, W. Skorupa, M. Helm, and S. Zhou, *Appl. Phys. Lett.* **105**, 042107 (2014).

37. R. Cheng, W. Wang, X. Gong, L. Sun, P. Guo, H. Hu, Z. Shen, G. Han, and Y-C. Yeo, *ECS J. Solid State Sci. Technol.* **2**, P138 (2013).
38. A. Claverie, S. Koffel, N. Cherkashin, G. Benassayag, and P. Scheiblin, *Thin Solid Films* **518**, 2307 (2010).
39. R. Koerner, I. A. Fischer, D. Schwarz, C. Clausen, M. Oehme, and J. Schulze, *Semicond. Sci. Technol.* **32**, 124005 (2017).
40. R. S. Nelson, *Rad. Effects.* **2**, 47 (1969).

Figure captions

Figure 1. The change of the Fermi energy position as a function of electron concentration in GeSn alloys containing 3.70 or 5.55 % of Sn calculated from the integrated density of states at 0K (a) and the band diagram in $Ge_{0.945}Sn_{0.055}$ with an effective carrier concentration of 3×10^{19} cm^{-3}.

Figure 2. The plot of $(\alpha h\nu)^2$ as a function of photon energy obtained from spectroscopic ellipsometry measurements (a). The inset in (a) shows the second derivative of the imaginary part of the dielectric function ($d^2\varepsilon_2(E)/dE^2$) around the E_0 transition obtained from undoped and n-type GeSn alloys after r-FLA. The position of the E_0 critical point as a function of Sn concentration extracted from the second derivative of the imaginary part of the dielectric function is displayed in (b) for an undoped and n-type layers. The inset in (b) shows the sheet resistance of undoped and P doped $Ge_{0.97}Sn_{0.03}$ samples as a function of temperature. (c) and (d) show the Hall resistance as a function of magnetic field measured at 3 K from undoped and P doped $Ge_{0.97}Sn_{0.03}$, respectively.

Figure 3. XRD θ–2θ scans around the Ge (004) diffraction of implanted and FLA treated samples with nominal 3 at.% of Sn (a) and 4.5 at.% of Sn (b). The insets in (a) and (b) show the Sn distribution in the alloys extracted from XRD data assuming a pseudomorphic GeSn layer. Reciprocal space maps around the (004) (c) and (e) and around (224) (d) and (f) reflections obtained from $Ge_{0.97}Sn_{0.03}$ and $Ge_{0.955}Sn_{0.045}$ samples, respectively. The orange circles in the images of the reciprocal space maps describe the expected theoretical positions of a fully relaxed and pseudomorphic Ge and GeSn lattice and the orange cross in (f) marks the position of a partially relaxed surface layer with $\varepsilon_{||}$= -0.26%.

Figure 4. Micro-Raman spectra of implanted and FLA treated samples with different Sn concentration.

Figure 5. RBS spectra obtained from virgin Ge and $Ge_{0.955}Sn_{0.045}$ alloy made by ion implantation and FLA.

Table 1. Fabrication parameter of GeSn alloy using ion implantation and flash lamp annealing.

Sample	Ion art	fluence	Sn concentration	Thickness of GeSn
Ge	-	-	-	
Ge:P	P	1×10^{15} cm^{-2}	-	
$Ge_{0.97}Sn_{0.03}$	Sn	1.2×10^{16} cm^{-2}	3%	60 nm
$Ge_{0.97}Sn_{0.03}$:P	Sn+P	$1.2\times10^{16}+1\times10^{15}$ cm^{-2}	3%	60 nm
$Ge_{0.965}Sn_{0.045}$	Sn	1.6×10^{16} cm^{-2}	4.5%	60 nm
$Ge_{0.965}Sn_{0.045}$:P	Sn+P	$1.6\times10^{16}+1\times10^{15}$ cm^{-2}	4.5%	60 nm

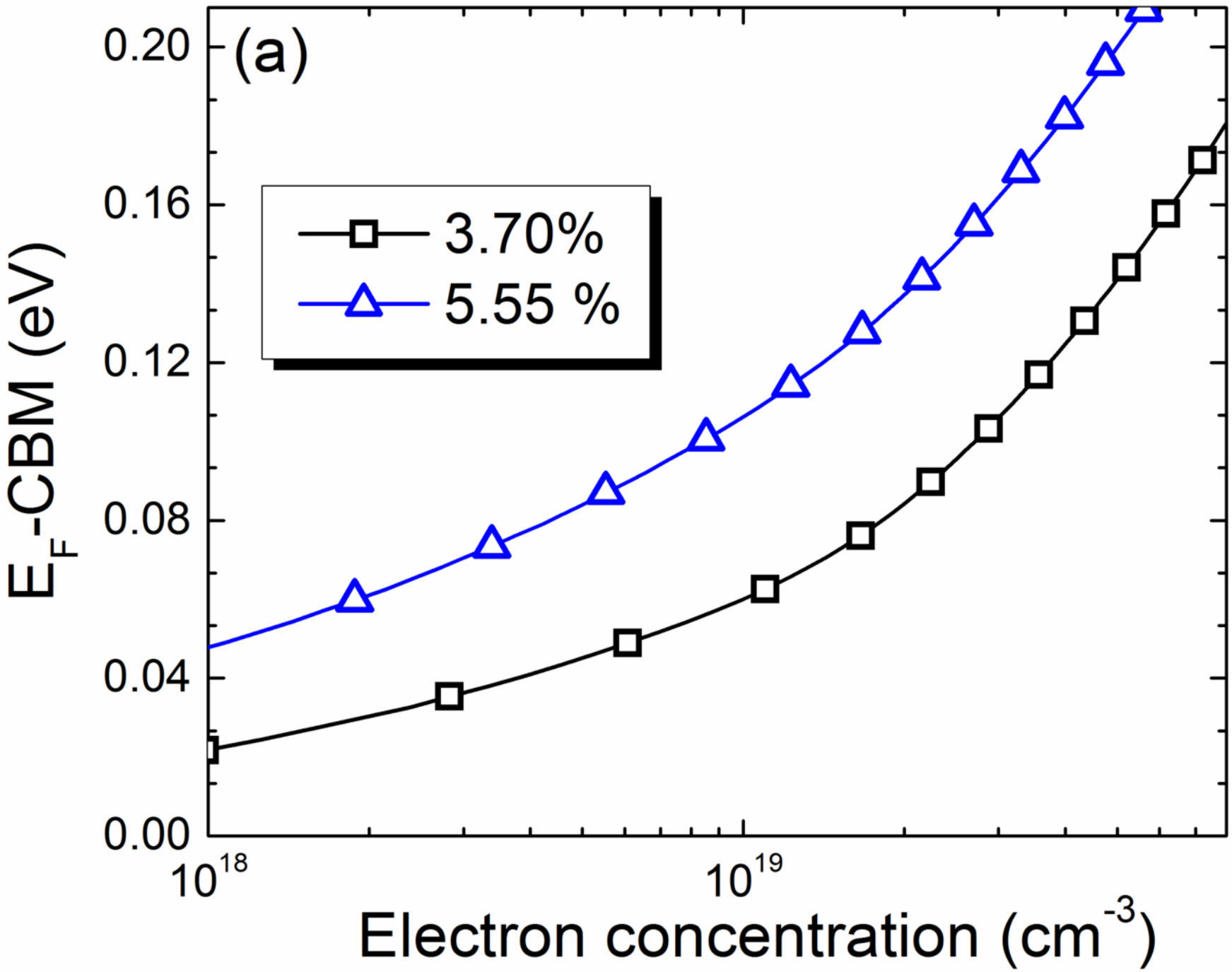
(a)
0.20
0.16
0.12
0.08
0.04
0.00
E_F-CBM (eV)
3.70%
5.55 %
10^{18}
10^{19}
Electron concentration (cm^{-3})

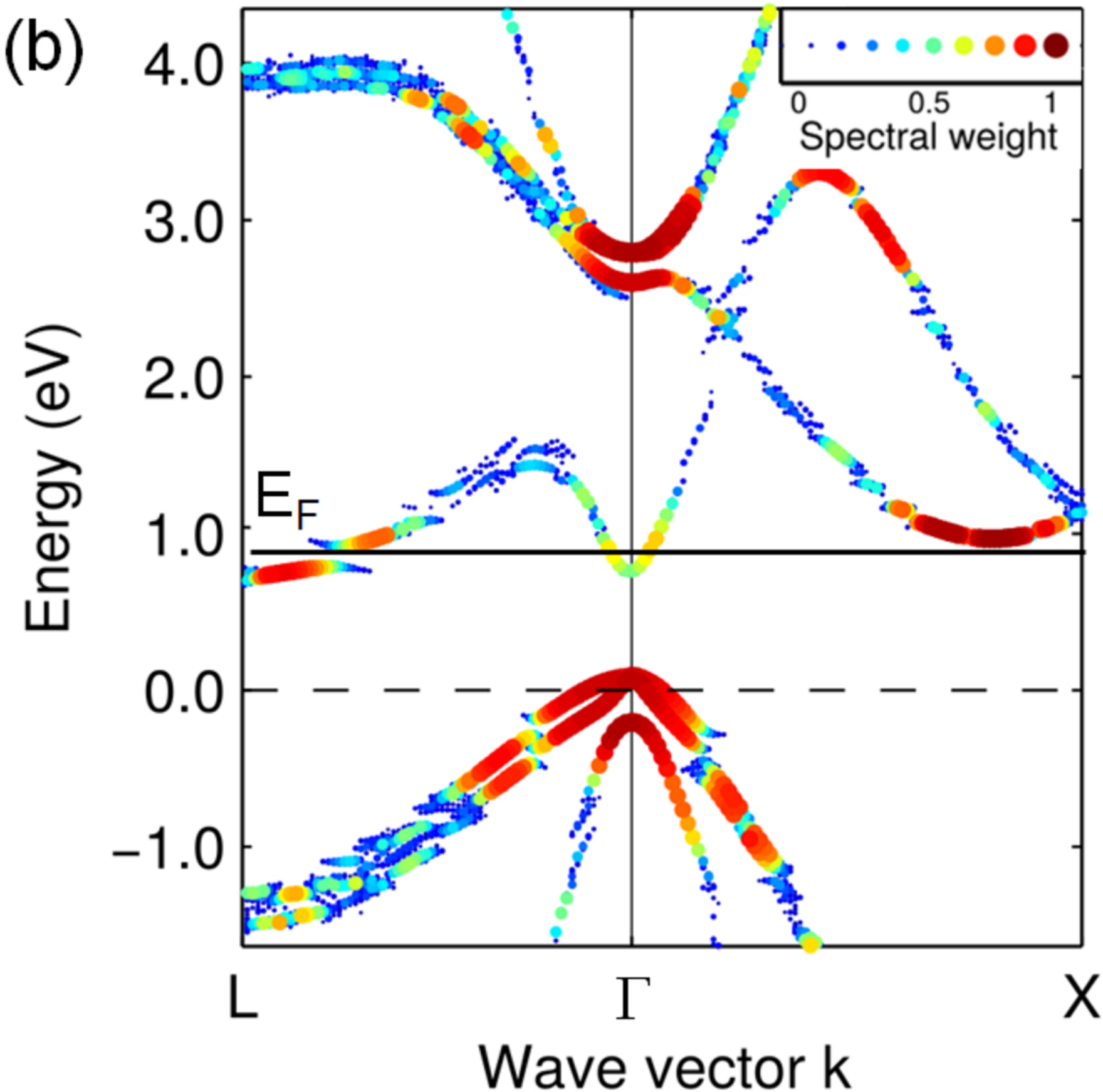
(b)
4.0
3.0
2.0
1.0
0.0
−1.0
Energy (eV)
E_F
0
0.5
1
Spectral weight
L
Γ
X
Wave vector k

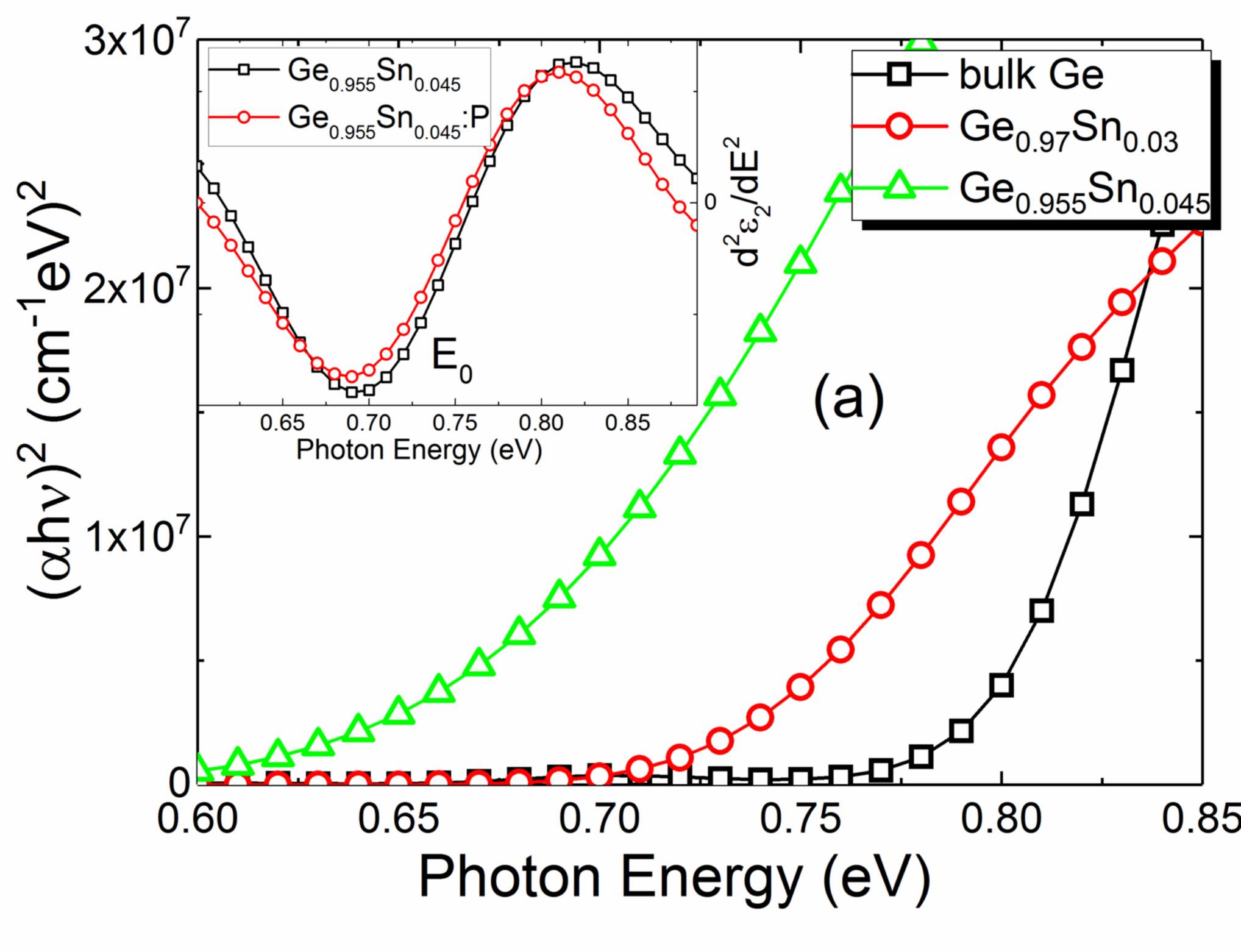
3x10^7
2x10^7
1x10^7
0
(αhν)^2 (cm^-1eV)^2
0.60
0.65
0.70
0.75
0.80
0.85
Photon Energy (eV)
bulk Ge
Ge0.97Sn0.03
Ge0.955Sn0.045
(a)
Ge0.955Sn0.045
Ge0.955Sn0.045:P
E0
d^2ε2/dE^2
0
0.65
0.70
0.75
0.80
0.85
Photon Energy (eV)

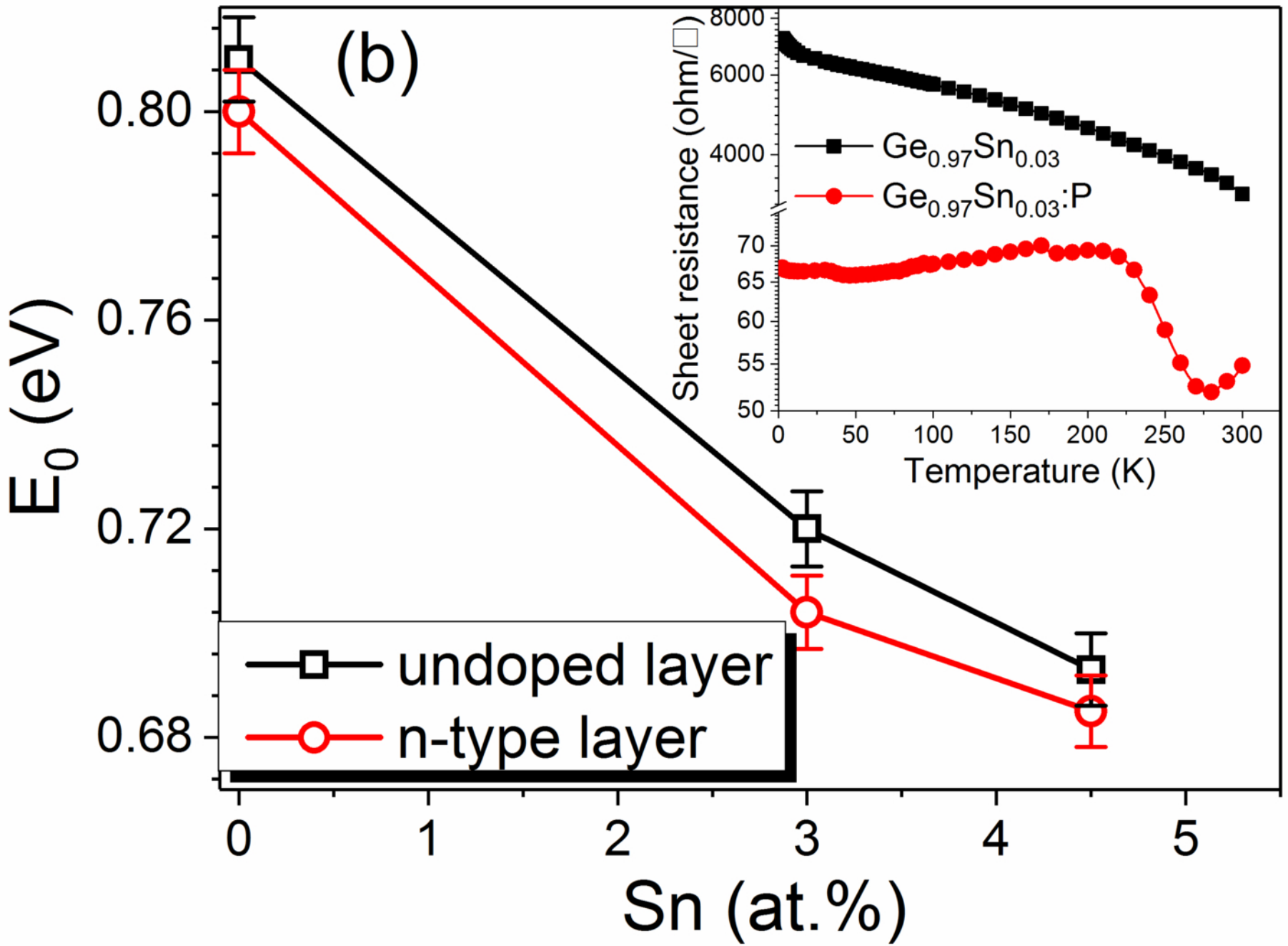
(b)
E_0 (eV)
0.80
0.76
0.72
0.68
0
1
2
3
4
5
Sn (at.%)
undoped layer
n-type layer
Sheet resistance (ohm/□)
8000
6000
4000
70
65
60
55
50
0
50
100
150
200
250
300
Temperature (K)
$Ge_{0.97}Sn_{0.03}$
$Ge_{0.97}Sn_{0.03}$:P

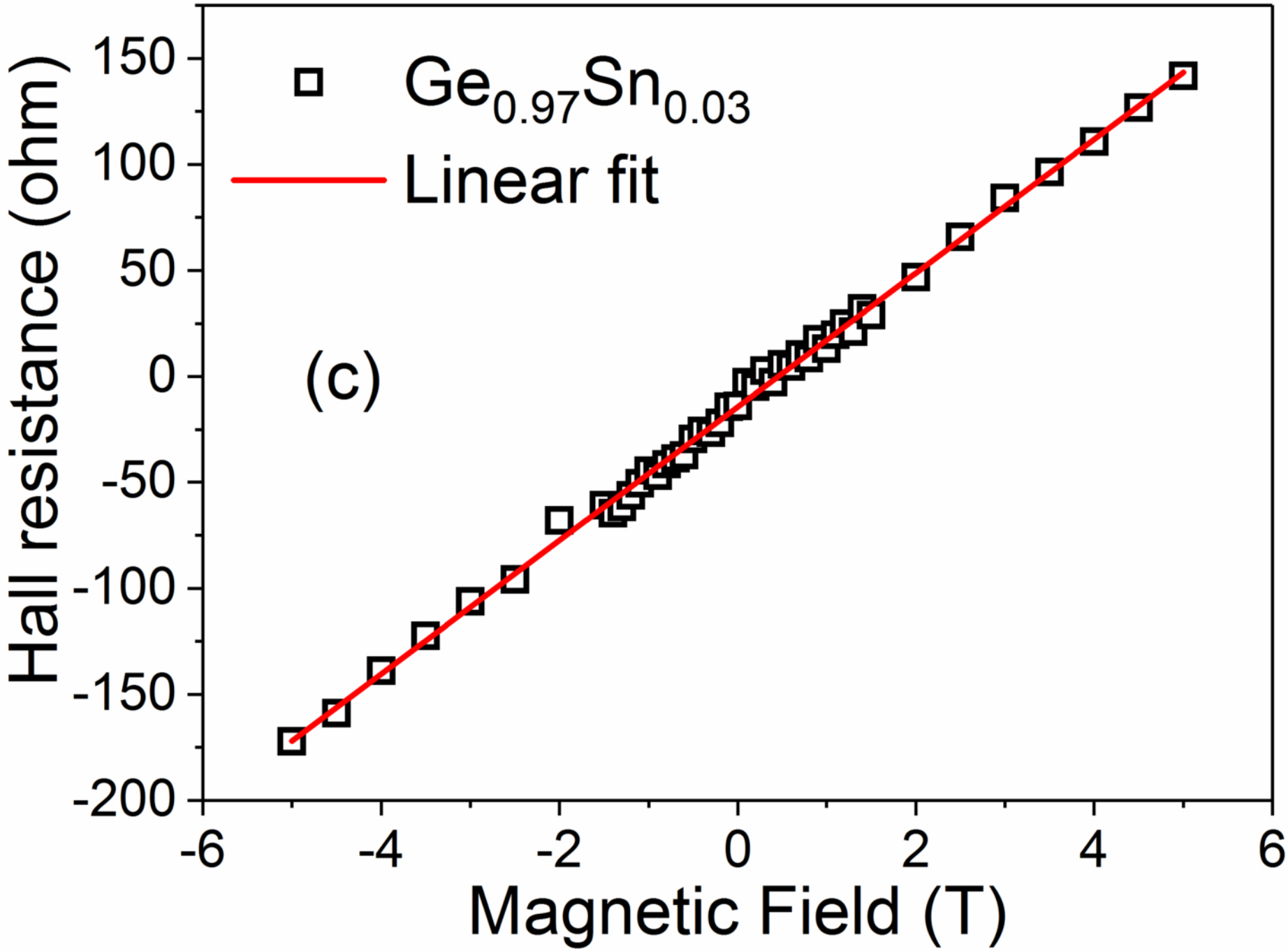
Ge0.97Sn0.03
Linear fit
(c)
Hall resistance (ohm)
Magnetic Field (T)
150
100
50
0
-50
-100
-150
-200
-6
-4
-2
0
2
4
6

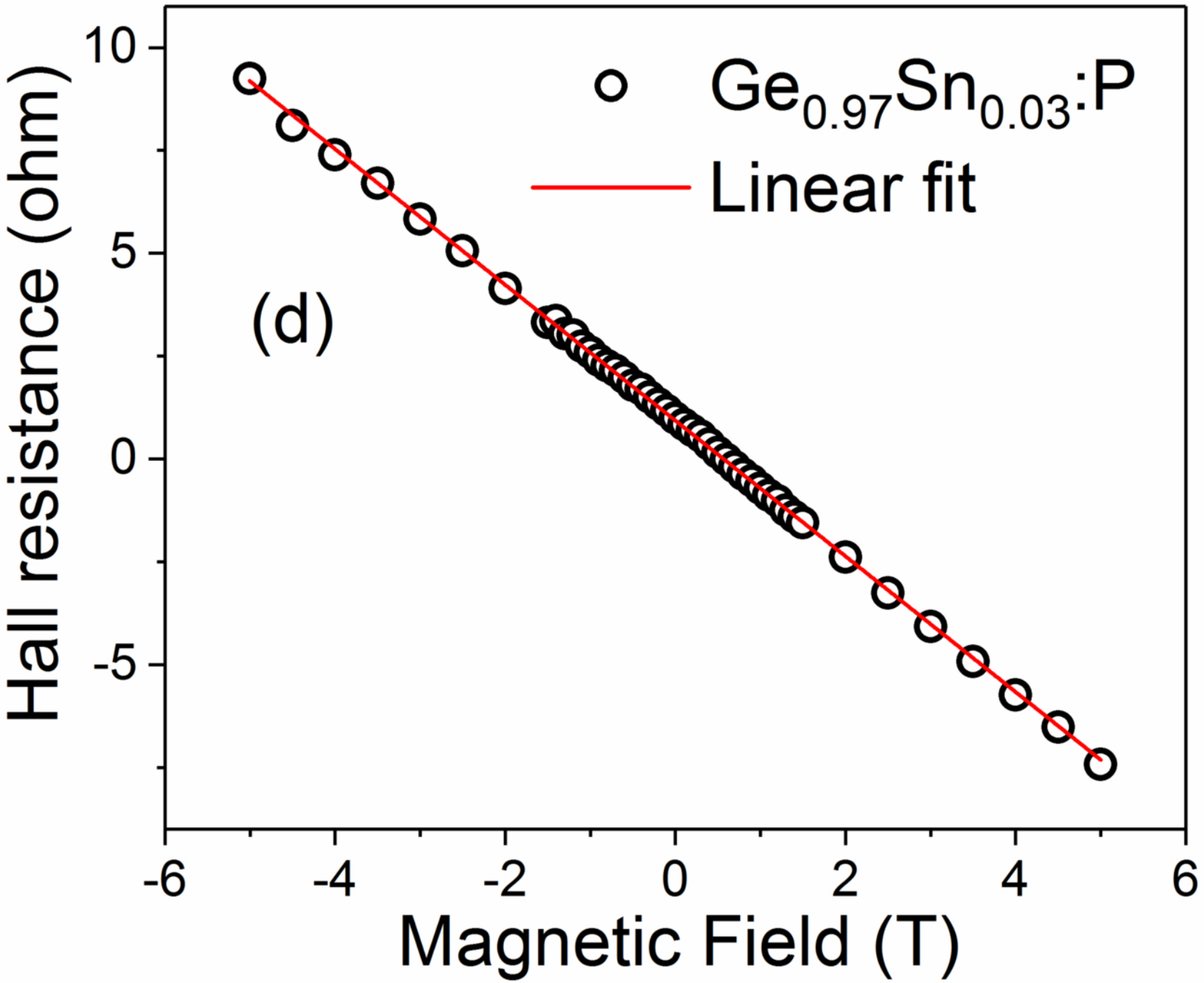
Hall resistance (ohm)
10
5
0
-5
-6
-4
-2
0
2
4
6
Magnetic Field (T)
(d)
Ge0.97Sn0.03:P
Linear fit

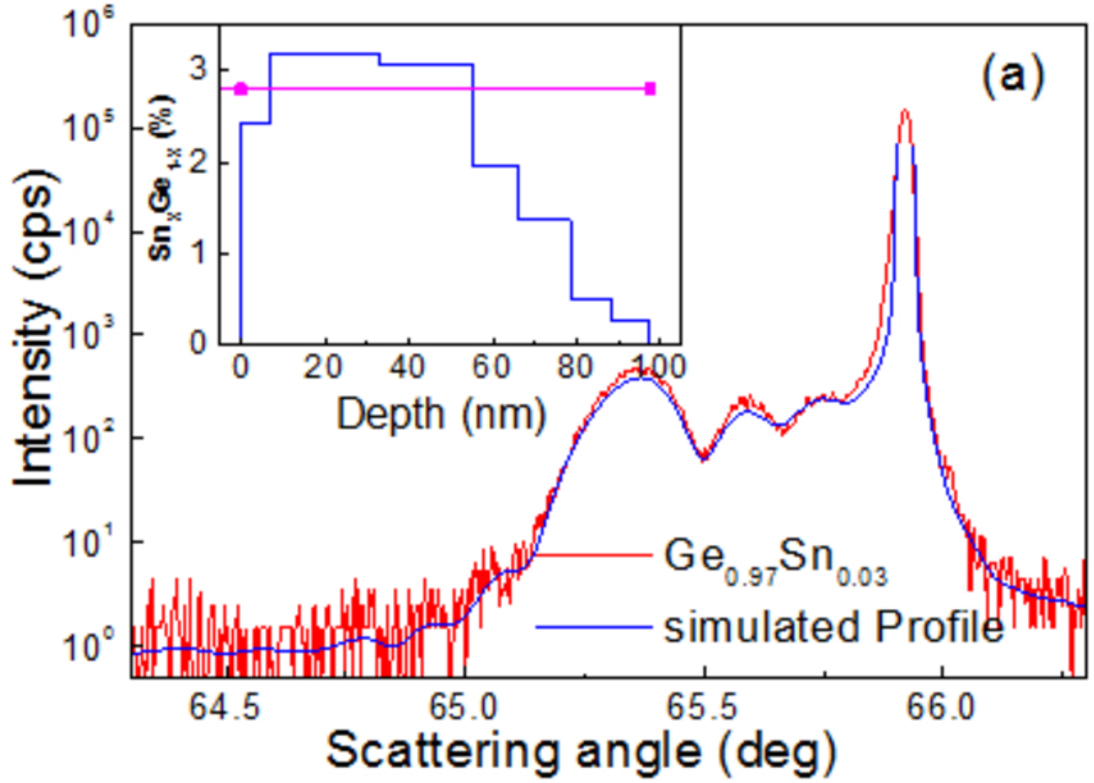
(a)
Intensity (cps)
Scattering angle (deg)
Depth (nm)
Sn_xGe_{1-x} (%)
$Ge_{0.97}Sn_{0.03}$
simulated Profile

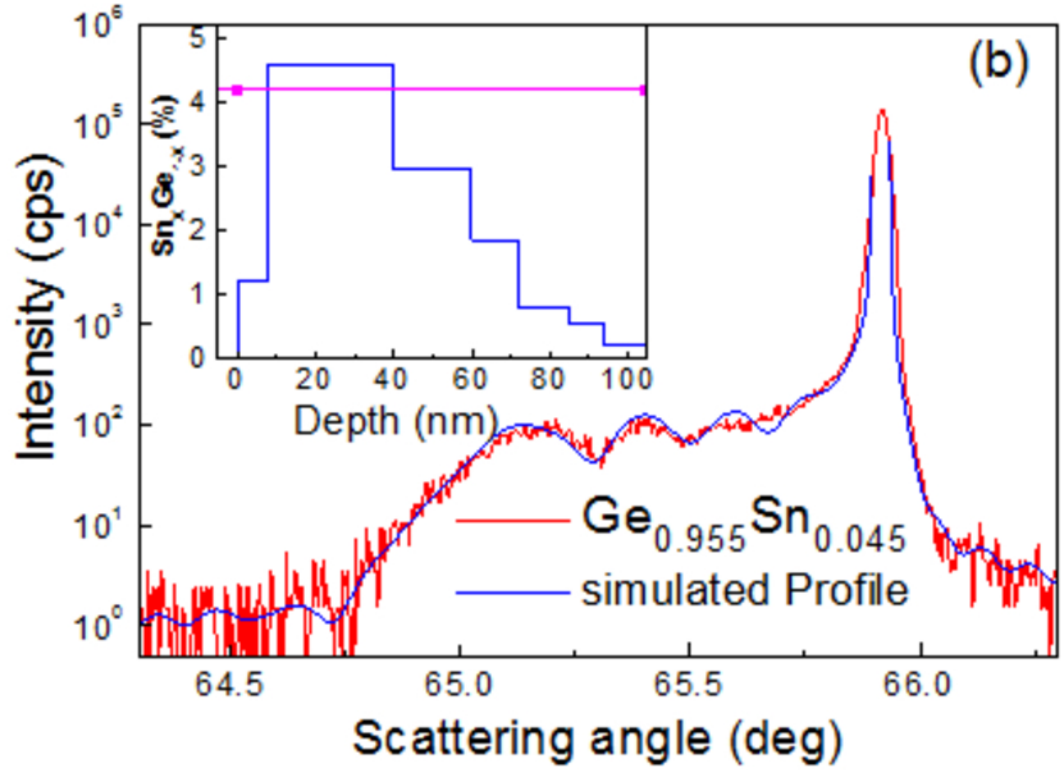
(b)
Intensity (cps)
Scattering angle (deg)
Depth (nm)
Sn_xGe_{1-x} (%)
$Ge_{0.955}Sn_{0.045}$
simulated Profile

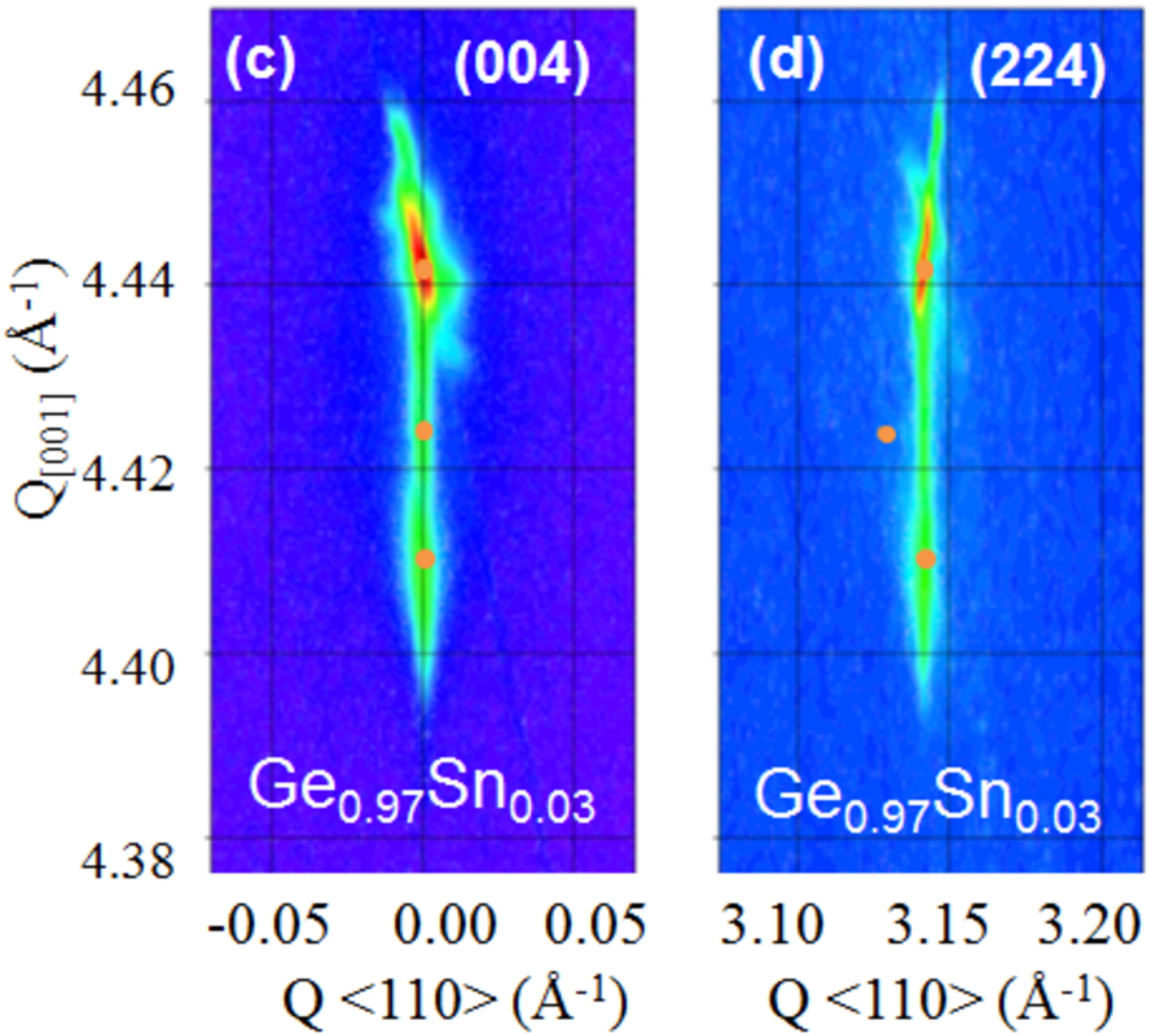
(c)
(004)
(d)
(224)
$Q_{[001]}$ (Å^{-1})
Q <110> (Å^{-1})
$Ge_{0.97}Sn_{0.03}$
$Ge_{0.97}Sn_{0.03}$

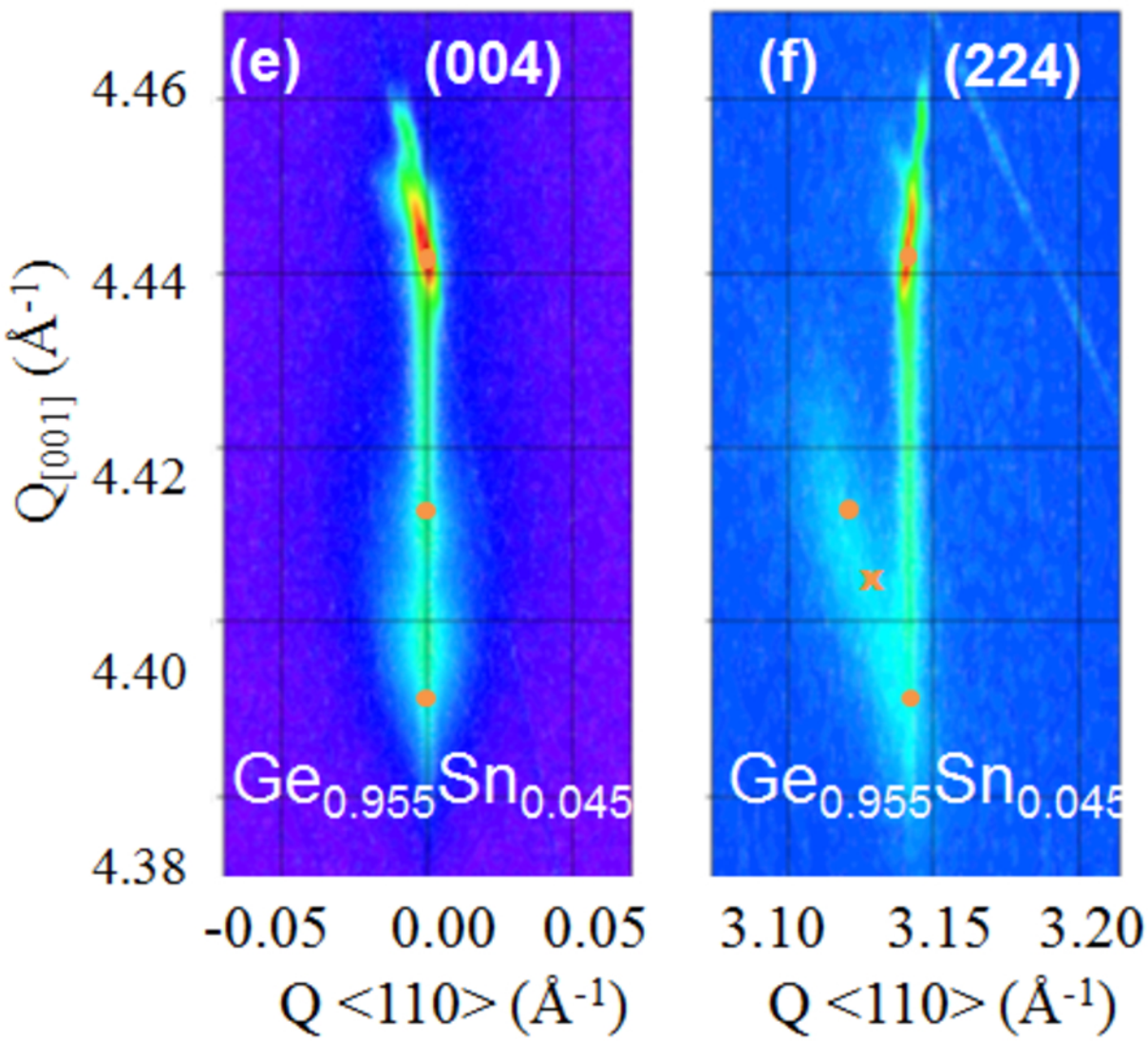
(e)
(004)
(f)
(224)
$Q_{[001]}$ (Å^{-1})
Q <110> (Å^{-1})
$Ge_{0.955}Sn_{0.045}$
$Ge_{0.955}Sn_{0.045}$

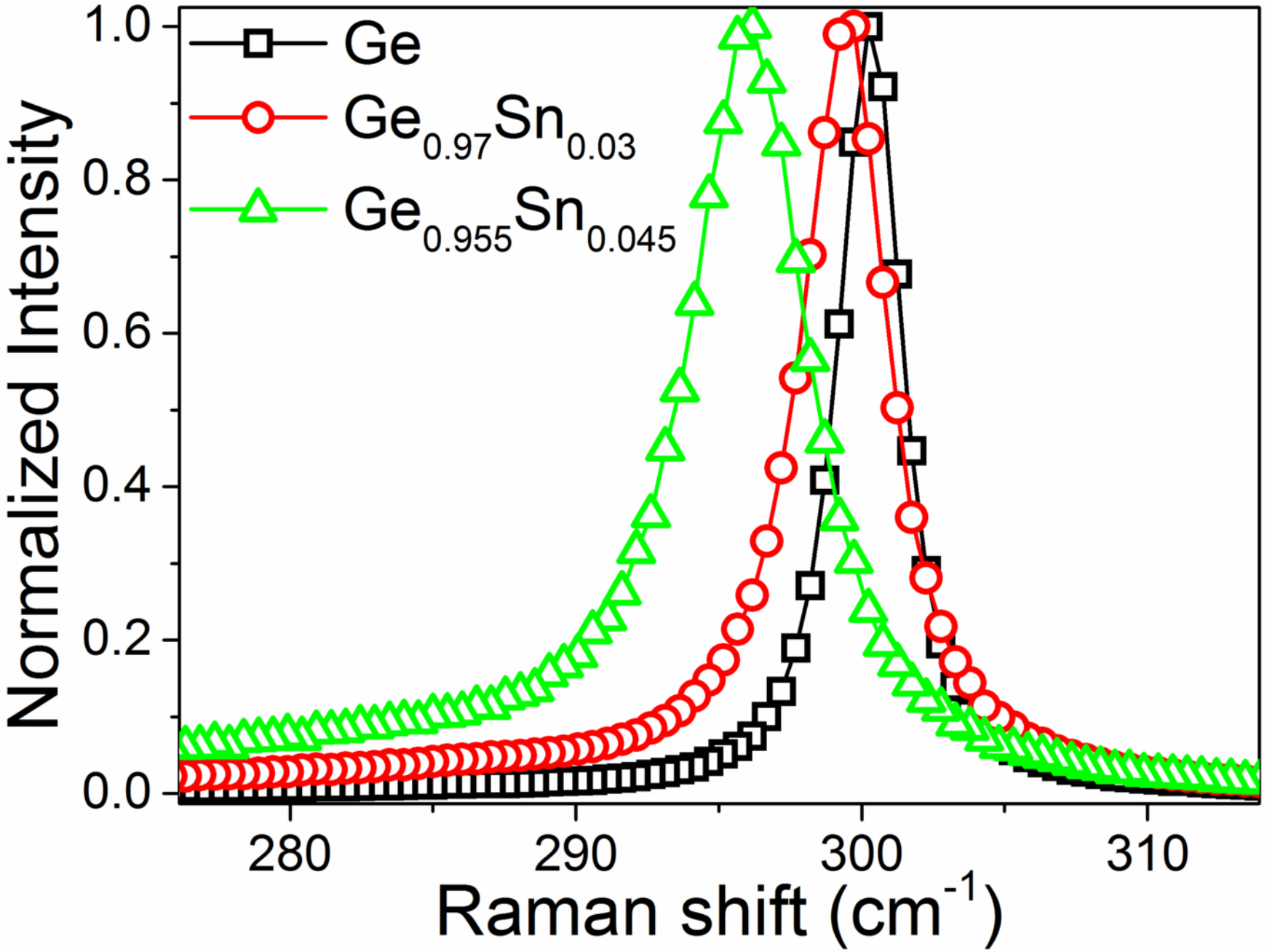
Ge
Ge0.97Sn0.03
Ge0.955Sn0.045
Normalized Intensity
1.0
0.8
0.6
0.4
0.2
0.0
280
290
300
310
Raman shift (cm-1)

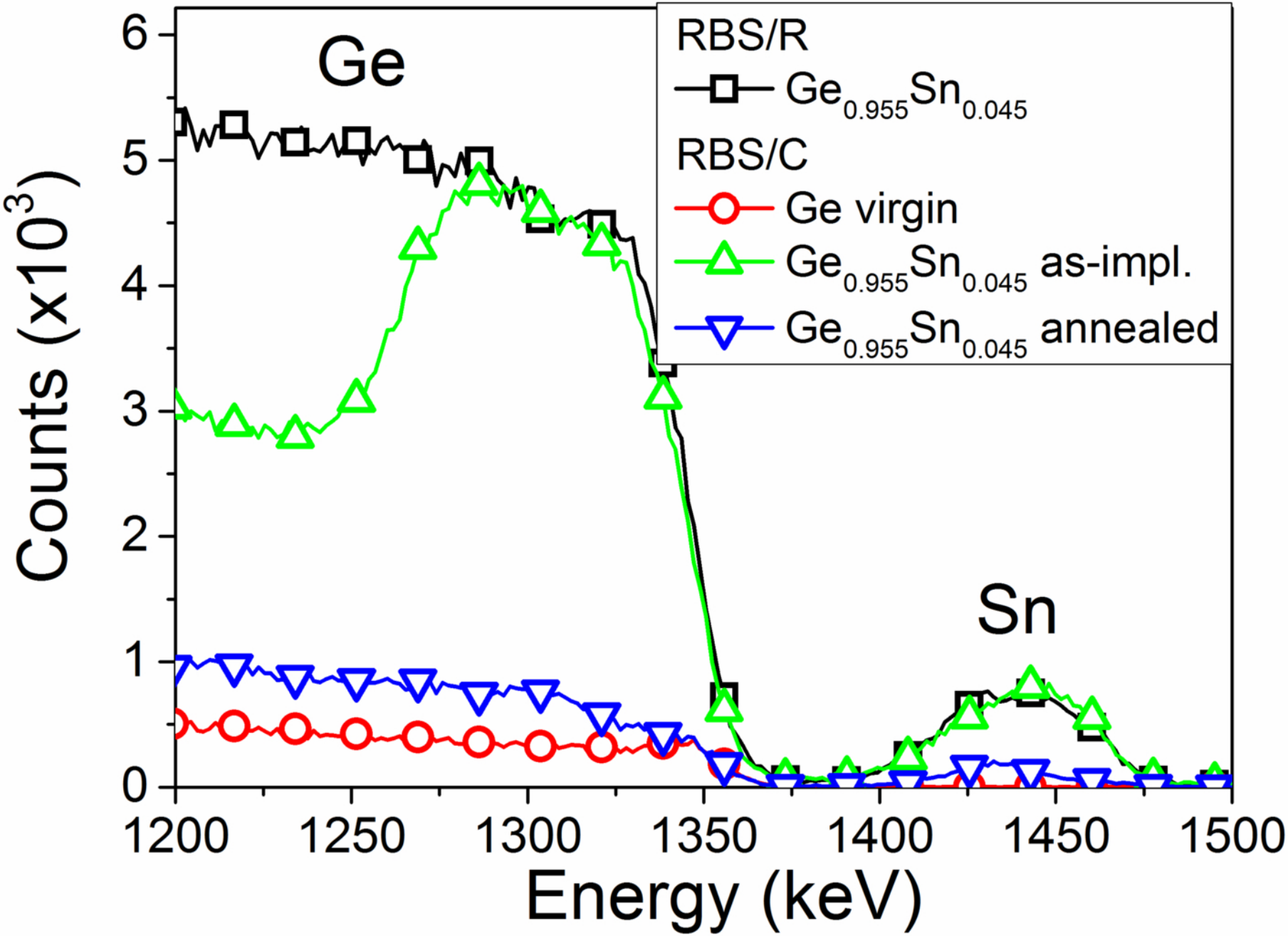
Ge
Sn
RBS/R
Ge0.955Sn0.045
RBS/C
Ge virgin
Ge0.955Sn0.045 as-impl.
Ge0.955Sn0.045 annealed
Counts (x10^3)
Energy (keV)
0
1
2
3
4
5
6
1200
1250
1300
1350
1400
1450
1500